Erschienen in: Experiments in Fluids ; 53 (2012), 5. - S. 1327-1333
https://dx.doi.org/10.1007/s00348-012-1362-9

Measurement of permeability of microfluidic porous media with finite-sized colloidal tracers

Christian Scholz · Frank Wirner · Yujie Li · Clemens Bechinger

Abstract We present two methods how the permeability in porous microstructures can be experimentally obtained from particle tracking velocimetry of finite-sized colloidal particles suspended in a liquid. The first method employs additional unpatterned reference channels where the liquid flow can be calculated theoretically and a relationship between the velocity of the particles and the liquid is obtained. The second method takes advantage of a time-dependent pressure drop that leads to an exponential decrease in the particle velocity inside a porous structure. From the corresponding decay time, the permeability can be calculated independently of the particle size. Both methods lead to results comparable with permeabilities derived from numerical simulations.

1 Introduction

Flow properties of liquids through porous media are of central importance in different areas, such as groundwater flow, environmental remedy, oil recovery, transport through biological tissue and microfluidic flow devices. However, due to the complexity of streamline distributions in random structures and the limitations of numerical and theoretical studies to investigate such processes on a wide range of length scales, flow properties are frequently described by semi-empirical laws obtained from macroscopic studies (Sahimi 1993). For a microscopic understanding of such processes, experiments within well-defined porous microfluidic devices are required, which allow a systematic investigation of liquid transport in different types of structures (Auset and Keller 2006).

For many applications, the most important macroscopic flow property is the permeability k, which connects the externally applied pressure ΔP with the flow rate Q according to Darcy's law:

$$Q = -\frac{kA}{\eta}\frac{\Delta P}{L}, \tag{1}$$

where A is the cross-sectional area of the porous medium, η the viscosity and L the length of the porous structure. In general, k depends on the detailed microstructure and thus on the precise flow field within the porous medium. Empirical relationships have been proposed, which relate the permeability to geometric and statistical properties of porous media, such as the porosity and the percolation threshold (Kozeny 1927; Carman 1937; Katz and Thompson 1986). In contrast to macroscopic systems where these parameters are not easily accessible, they can be directly measured in man-made porous structures, for example, within microfluidic devices. Even then, however, the accurate determination of flow properties within such samples remains a challenging task as pointed out below.

One method to visualise the fluid's flow field is particle tracking velocimetry (PTV) where colloidal particles are used as tracers (Santiago et al. 1998). Yet, in contrast to ideal tracers that would perfectly follow the flow, colloidal

Christian Scholz and Frank Wirner contributed equally to this publication.

C. Scholz (✉) · F. Wirner (✉) · Y. Li · C. Bechinger
Physikalisches Institut, Universität Stuttgart,
70569 Stuttgart, Germany
e-mail: c.scholz@physik.uni-stuttgart.de

F. Wirner
e-mail: f.wirner@physik.uni-stuttgart.de

C. Bechinger
e-mail: c.bechinger@physik.uni-stuttgart.de

particles often strongly deviate from such conditions due to their finite size, mass and additional interactions with the porous matrix. In general, tracer particles should be significantly smaller than the shortest relevant hydrodynamic length scale (Lindken et al. 2009). This, however, is often difficult or even impossible to achieve, for example, in random porous media with a broad range of length scales. In addition, deviations from fluid flow lines due to inertial effects can occur even for small particles, as recently shown for time-periodic and chaotic flows (Ouellette et al. 2008; Pushkin 2011). Consequently, the impact of particle size within inhomogeneous flow fields has to be considered, which leads to relevant hydrodynamic effects even in simple geometries (Segre and Silberberg 1962; Staben et al. 2003).

In this paper we demonstrate how the permeability of porous structures can be obtained by PTV measurements independently of the particle size. In contrast to well-established techniques for permeability measurements which employ constant flow rates provided by syringe pumps, our methods are also applicable for measuring permeabilities in small samples with very low flow rates.

The paper is organised as follows: In Sect. 2 we present our experimental PTV set-up. Section 3 discusses the tracer behaviour in a thin microfluidic channel, in particular the relation between the mean particle velocity $\bar{u}$ and the mean fluid velocity $\bar{v}$. Section 4 illustrates the complexity of particle transport and the impact on PTV measurements inside a porous structure. Finally, the two methods for permeability measurement are presented and compared in Sect. 5. A concluding summary is given in Sect. 6.

2 Experimental set-up

We prepared different types of microfluidic channels with height h in the range of 5–20 μm, width $w = 1$ mm and length L between 8 and 9 mm. The devices are made by soft lithography, which allows the fabrication of structures with different porosity and morphology (Quake and Scherer 2000). A hydrostatic pressure ΔP is applied to the channels by connecting two reservoirs to the in- and outlet and varying the levels of injected liquid. To ensure that ΔP remains constant during a measurement, the cross-sectional areas of the reservoirs are chosen to be sufficiently large. Polystyrene particles of different diameters d in the range of 1.2–5.2 μm are injected into the solvent, which flows through the structure. The samples consist of three segments, as illustrated in Fig. 1. The inner segment contains a porous structure of randomly overlapping circles created by a numerical algorithm, and the two outer segments connect the structure to the reservoirs. The porosity ϕ is defined as the volume fraction of the fluid phase within the

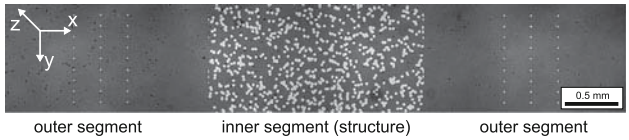

Fig. 1 Photograph of a typical microfluidic device composed of a porous segment (*middle*) created by randomly overlapping circles. The *inner part* is connected to two plain outer segments

structure. Size-dependent averaged particle velocities $\bar{u}(d)$ are determined from the ensemble average over all particles of the same diameter d within the field of view (400×300 μm^2). All experiments were performed at room temperature (20 °C).

The experimental goal is to determine the permeability k_{por} of the inner, that is, porous part of a microfluidic device. This can be achieved by determining the flow rate Q for a given ΔP, from which the permeability k_{tot} of the entire sample can be calculated using Eq. 1. k_{por} is then determined by considering the sample segments as a series of hydraulic conductivities. For ideal tracers where the mean particle velocity $\bar{u}$ and the mean fluid velocity $\bar{v}$ are identical, Q can then be determined from a PTV experiment because for an incompressible fluid the continuity equation implies

$$Q = \bar{v} A \phi. \tag{2}$$

Therefore, we analyse whether particles of different diameter can be indeed considered as ideal tracers in the following section.

3 Mean particle and mean fluid velocity in simple geometries

At first we discuss the behaviour of tracers in a plain non-porous microfluidic channel ($\phi = 1$) of length $L = 8{,}600 \pm 50$ μm and height $h = 6.5 \pm 0.3$ μm. Here, the flow field is known to be parabolic in z-direction, constant in x-direction and zero in y-direction (Bruus 2007), as illustrated in Fig. 2. For this simple geometry the permeability is given by $k = h^2/12$ (Bruus 2007).

We apply a pressure drop $\Delta P = 479$ Pa which results in a mean fluid velocity $\bar{v} = 196 \pm 20\,\mu\mathrm{m/s}$, according to Eq. 1. When comparing $\bar{u}(d)$ for different particle diameters, we find a decreasing $\bar{u}$ in dependence of d, as shown in Table 1. The differences in $\bar{u}$ amount up to 26 %, which clearly demonstrates that the particles are far from being ideal pointlike tracers and that $\bar{u}$ is not identical to $\bar{v}$ (Taylor 1953).

Several reasons for this difference exist: (1) non-uniform particle height distribution $p(z)$ of the particles inside the channel mainly due to gravitational forces and (2)

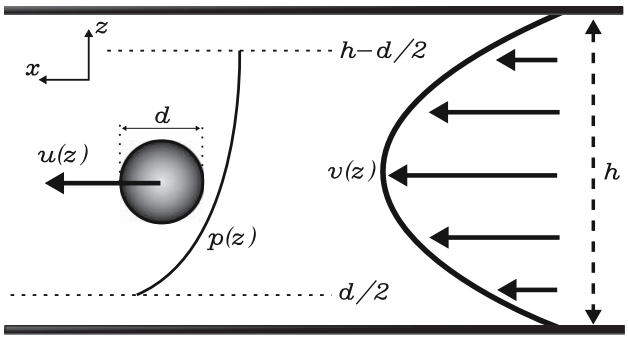

Fig. 2 Illustration of a particle with diameter d in the x/z-plane inside a channel of height h. The particle is moving with local particle velocity $u(z)$ in a parabolic flow profile $v(z)$ of the liquid. Due to the finite mass of the particle, the probability distribution $p(z)$ is non-uniform

Table 1 Mean particle velocity $\bar{u}$ and calculated $\tilde{u}$ for different-sized polystyrene particles of diameter d within an empty channel of height $h = 6.5 \pm 0.3$ μm, length $L = 8{,}600 \pm 50$ μm and the corresponding gravitational length λ

d (μm)	$\bar{u}$ (μm/s)	$\tilde{u}$ (μm/s)	λ (μm)
1.2	270.6 ± 1.4	240 ± 36	8.75
2.4	246.6 ± 3.3	224 ± 32	1.09
3.4	234.3 ± 4.6	194 ± 32	0.383
5.2	215.7 ± 3.6	176 ± 59	0.107

The mean fluid velocity is calculated to be 196 ± 20 μm/s

hydrodynamic interactions between the particles and the walls which lead to a reduced particle velocity $u(z)$ (compared to $v(z)$). In particular for large particle sizes and at small particle–wall distances, this effect can be sizeable as has been demonstrated (Staben et al. 2003). Finally (3) the limited field of view leads to a biased sampling of high particle velocities since faster particles pass more frequently than slow particles and thus shift $\bar{u}$ to higher values.

To estimate the mean particle velocity for a given d, we have assumed a Boltzmann particle height distribution $p(z) = \exp(-z/\lambda)$ which is characterised by the gravitational length $\lambda = \frac{k_B T}{m_p g}$, where k_B is the Boltzmann constant, T is the temperature, m_p is the particles' effective mass, and g is the gravitational acceleration (Frenkel 2002). In addition, hydrodynamic effects were approximated by the numerical results given in reference (Staben et al. 2003). The resulting theoretical $\tilde{u}(d)$ for m_p calculated according to the density of PS ($\rho = 1.05$ g/cm^3) is also shown in Table 1 (see Appendix 1 for a full derivation of $\tilde{u}(d)$). The obtained values of $\tilde{u}$ are close to $\bar{u}$ and show a similar dependence on d. One reason for the quantitative discrepancy is that a Boltzmann distribution is certainly too simple to describe the particle distribution in the presence of a flow. A more accurate model should also include electrostatic interactions which would push the particles away from the walls and thus towards faster streamlines.

4 Particle transport in porous structures

In a random porous structure the streamline distribution becomes even more complex, and the flow field cannot be determined analytically. To illustrate the particle transport through a porous sample, in Fig. 3 we show typical particle trajectories within a porous microstructure ($\phi = 0.82$) for two colloidal species with diameter 1.2 μm and 5.2 μm at $\Delta P = 479$ Pa.

As can be seen, there is a strong dependence of the particle trajectories on the particle size, which is largely caused by volume exclusion due to hard core interactions between the particles and the porous matrix. This leads to faster transport of larger colloids through constricted regions since their centre of mass is further away from the matrix surfaces (Auset and Keller 2004). Additionally, hard core repulsion leads to the displacement of particles perpendicular to streamlines (streamline crossing), which breaks the time-reversibility of particle trajectories even in the Stokes limit (Loutherback et al. 2009). As a result large particles cannot access the entire region behind obstacles as exemplarily shown in Fig. 3c–f. This effect depends on the ratio of obstacle and tracer diameter and becomes most pronounced for size ratios around one as illustrated in Fig. 3f where a sticking 5.2 μm particle acts as an obstacle for other tracers of identical size. This kind of volume exclusion is counteracted by Brownian motion, but it persists up to low Péclet numbers. Furthermore, large particles, owing to their small diffusion constant, cannot diffuse into stagnant parts if the Péclet numbers of the surrounding regions are too high.

We also performed an analysis of the local ensemble average particle velocity $\bar{u}(x, y)$ by dividing the field of view into small cells and calculating the average velocity (2D-projection) of particles in each cell via a MATLAB program. Figure 4 shows the resulting velocity fields. From these data we obtained the spatially resolved average particle velocity $\bar{u}(x, y)$ which is shown in Fig. 4 for particles with $d = 1.2$ and 5.2 μm. As expected, the particles are fastest (yellow) in regions where nearby obstacles form constrictions with an increased fluid flow velocity and are slower far away from obstacles (red). Similarly as in the experimentally determined particle trajectories, the calculated velocity fields quantitatively differ for the two particle sizes as, for example, seen by the larger area of excluded volumes (black regions) around the obstacles. Since even for a simple non-porous channel a relationship between $\bar{u}$ and $\bar{v}$ cannot be determined, it is obvious that the

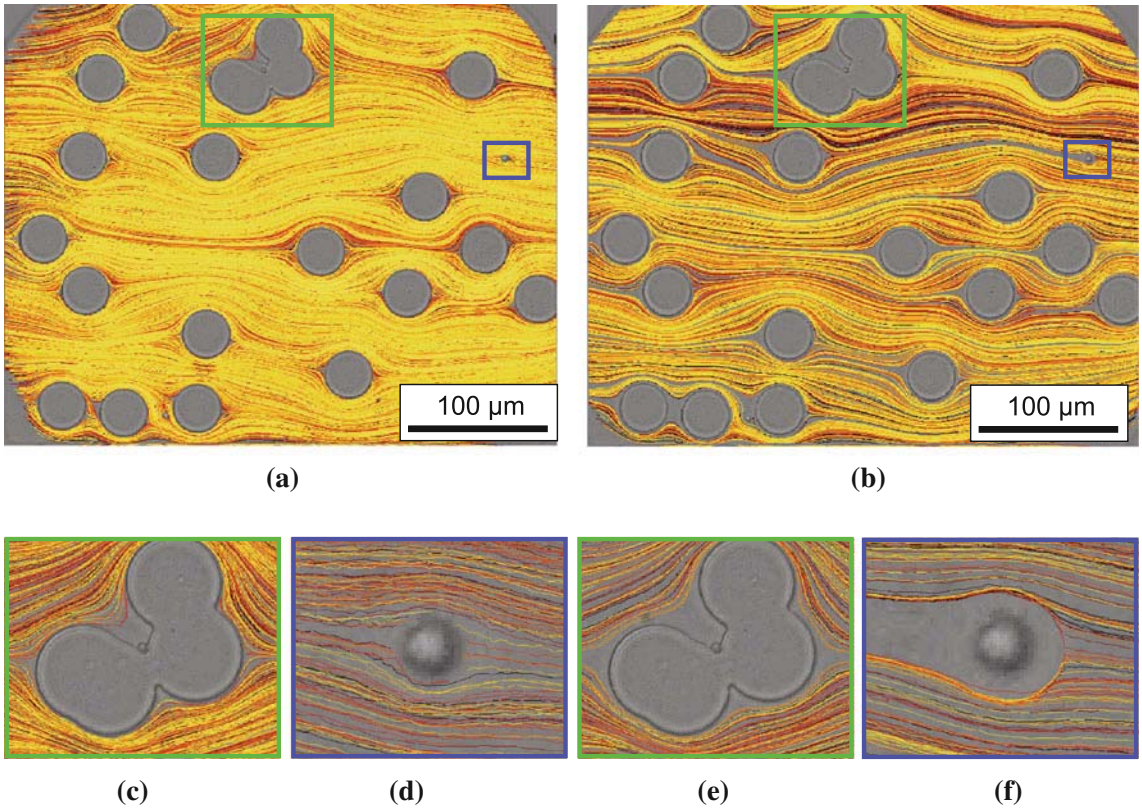

Fig. 3 Particle trajectories within a porous structure for 1.2 µm (**a**) and 5.2 µm (**b**) particles. The flow direction is from right to left. The colour code is chosen arbitrarily to distinguish individual trajectories. **c**, **d** Small tracers sample the velocity field close to the obstacles but are still excluded significantly from stagnant parts. **e** Large tracer particles are excluded from stagnant parts even if the length scale is larger than the particle diameter. **f** A sticking 5.2-µm particle leads to a pronounced volume exclusion for large particles

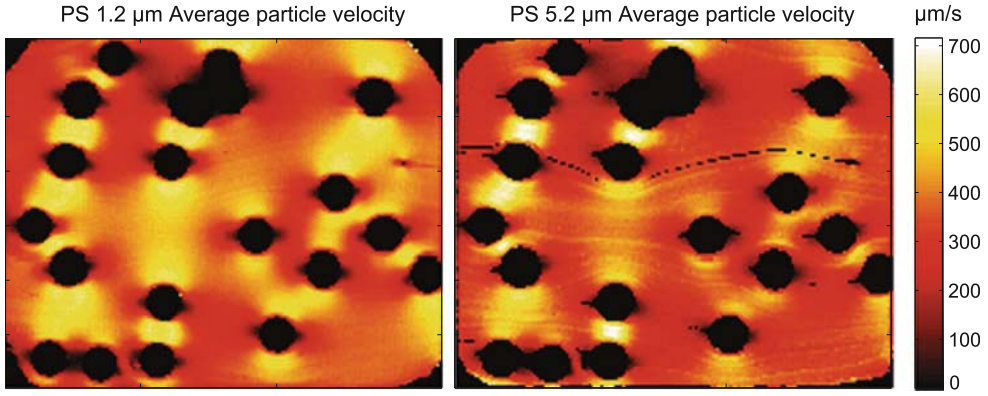

Fig. 4 Colour-coded spatially resolved average particle velocity for a pressure drop $\Delta P = 479$ Pa for $d = 1.2$ µm and 5.2 µm PS particles. The field of view was divided into 160 × 128 cells, and the average particle velocity is calculated from the ensemble average over all trajectories within each cell

situation is even worse for a random porous structure and it might appear that the experimental measurement of the permeability based on PVT is impossible. Consequently, reference measurements in the outer segments have to be performed in order to determine the flow rate. Using our previous results, the two possible techniques of measuring k_{por} from the tracer motion are explained in the following section.

5 Experimental determination of the permeability

5.1 Constant-head method

In order to measure k_{por}, we need to determine the flow rate that is related to the mean fluid velocity $\bar{v}$ according to Eq. 2. However, as has been shown in Sect. 3, $\bar{u}$ is not identical to $\bar{v}$ even for simple channel geometries. Nevertheless, both quantities are in close relationship as shown in Fig. 5 where the mean particle velocities for different particle sizes are plotted as a function of ΔP both for the inner, porous segment and for the outer plain segments. In combination with Eq. 1, the linear relationship between $\bar{u}$ and ΔP suggests that $\bar{u} = c_d \cdot \bar{v}$, where c_d is a constant for a given particle diameter d.

To determine the value of c_d, we measure $\bar{u}$ inside an unpatterned reference channel of rectangular cross section of known geometry where $\bar{v}$ is known analytically. Assuming that c_d is the same within the outer segment of the sample, we can determine $\bar{v}$ from a measurement of $\bar{u}_d$, which enables us to calculate the total permeability of the sample.

For an experimental realisation of such a measurement, we added two unpatterned reference channels to our sample as shown in the inset of Fig. 6. Within such a microfluidic device, we can at the same time determine the mean particle velocity of the unpatterned reference channels and that of the test channel containing the porous structure at the same pressure drop. With the procedure outlined above, this eventually leads to the determination of k_{por} for arbitrary structures. A remaining problem is that the theoretical flow rate of the outer segments enters this calculation, so that the technique shows poor accuracy for high-porosity structures that have about the same permeability as the outer segments. This is similar to an electrical resistance measurement where the resistance of the leads is comparable to the resistance being measured.

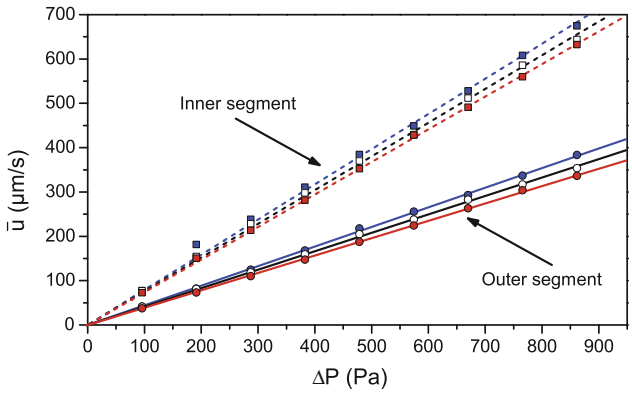

Fig. 5 Comparison of mean particle velocities $\bar{u}$ in non-porous (*circles*) segment and a representative part of the inner segment (*squares*) for $d = 1.2$ μm (*blue*), 2.4 μm (*white*) and 3.4 μm (*red*) particles as a function of the applied hydrostatic pressure ΔP. The *solid* and *dashed lines* correspond to linear fits

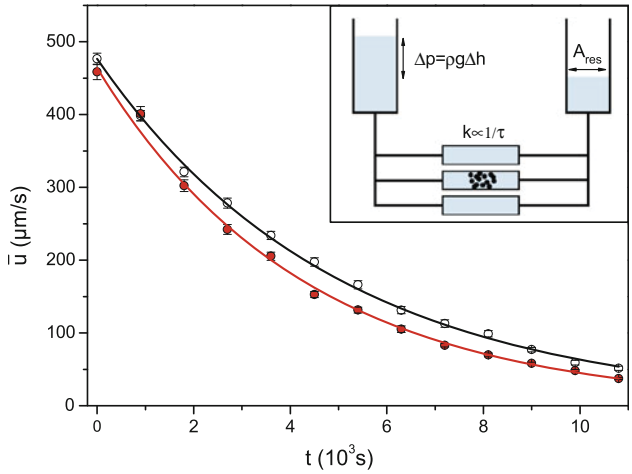

Fig. 6 Time dependence of the mean particle velocity $\bar{u}$ for an exponentially decreasing pressure drop for 2 μm (*white*) and 3 μm (*red*) particles inside the outer segment. The permeability of the whole structure can be deduced from the decay time constants $\tau = 4{,}212 \pm 68$ s and $4{,}701 \pm 108$ s, respectively. The inset shows a schematic of the set-up. Two reservoirs with cross-sectional area A_{res} are connected to the microstructure that consists of three parallel channels. The middle channel contains a porous structure of randomly placed overlapping *circles* with permeability k_{por}

5.2 Falling-head method

To determine the permeability of a porous microstructure independently of any theoretical input parameters and independently of the tracer size in a PTV measurement, we introduce an alternative concept which is also known at macroscopic scales (Marshall et al. 1996) and makes use of the fact that the pressure drop ΔP is related to an excess volume V. The change of the excess volume caused by fluid flowing through the sample results in an exponential decrease in ΔP, similarly to the discharge of a capacitor across a resistance. Using that $\bar{u} \propto \Delta P$ this leads to a decreasing particle flow velocity as a function of time

$$\frac{d}{dt}\bar{u} = -\tau^{-1}\bar{u}, \tag{3}$$

which does not depend on the particle size and where $\tau \propto k^{-1}$ (see Appendix 2 for a full derivation). It should be realised that Eq. 3 is valid independently whether the particle velocities are obtained inside the porous part or the outer segments of the sample (cf. Fig. 1). Only stagnant parts where Brownian motion plays a major role should be avoided. It should be noted that the liquid flow velocity through a porous sample could in principle also be determined by the falling level of a water column; however, due to the small flow rates in microscopic samples, this would

require rather long observation times. Because mean particle velocities can be almost instantly observed with PTV measurements, such an approach is rather preferred.

5.3 Results and comparison

To compare both methods, we used a microstructure ($\phi = 0.91$, $h = 19.0 \pm 0.3$ μm, length $L = 8{,}150 \pm 50$ μm) where the flow rate is in a regime which allows us to use the falling-head (FH) and the constant-head (CH) method. The constant-head measurement was carried out as previously described. In order to realise a sizeable variation in the applied pressure during the falling-head measurement, we reduced the cross-sectional area of the reservoirs A_{res} to 0.176 cm^2. The resulting exponential decrease in $\bar{u}$ for particles with $d = 2$ and 3 μm in the outer segment of the middle channel is shown in Fig. 6. From a fit with Eq. 3 we obtain decay-times $\tau = 4{,}212 \pm 68$ s and $\tau = 4{,}701 \pm 108$ s for the smaller and larger particles, respectively. From these values we calculate k_{tot} and the permeability k_{por} of the porous part of the sample for the two different decay-times.

The resulting values for the total permeability k_{tot} and the permeability of the porous inner part k_{por} are summarised in Table 2. The values for k_{tot} obtained by the two different methods differ by 12 %, which shows that either method provides accurate results. For comparison we also performed a finite-element simulation of incompressible Stokes flow for the structure with COMSOL, which is in agreement with the experimental results and demonstrates that both methods give indeed reliable results. The higher deviations of the values for k_{por} are mainly caused by the fact that the porous part is very small compared to the whole sample.

The advantage of the falling-head method is that the outer segments and the reference channels can be removed completely. However, for low-porosity structures and low flow rates, this method suffers from longer measurement times. This restricts the applicability to structures with $k_{\text{por}} \geq 0.3 \times 10^{-11}$ m^2. In general, it is possible to extend that range by making A_{res} smaller. In the case of lower permeabilities, the constant-head method should be preferred, even though it may suffer from simplifications such as the assumption of a perfectly rectangular channel and the additivity of outer segment permeability and structure permeability. This method yields accurate results for structures with $k_{\text{por}} \leqslant 1.8 \times 10^{-11}$ m^2. For either method the range of permeability for which precise measurements can be performed can be extended by making the microstructure larger.

Table 2 Comparison of the total permeability k_{tot} and permeability of the porous inner part k_{por} of a microstructure of height $h = 19.0 \pm 0.3$ μm, length $L = 8{,}150 \pm 50$ μm and porosity $\phi = 0.91$

	CH	FH 2 μm	FH 3 μm	Simulation
k_{tot} (10^{-11} m^2)	2.67	2.91	2.60	N/A
k_{por} (10^{-11} m^2)	1.58	2.07	0.81	1.74

For the constant-head measurement we used both particle species

6 Conclusions

In summary, we introduced two methods how the permeability k_{por} of porous microstructures can be determined from a PTV measurement using a dilute suspension of finite-sized colloidal tracers. We showed that small colloids are not necessarily ideal tracers since the mean particle velocity $\bar{u}$ can differ substantially from the mean fluid velocity $\bar{v}$. Hence, a direct measurement of $\bar{v}$ is not feasible. The first approach, that is, the constant-head technique, requires additional unpatterned reference channels with rectangular cross section where the liquid flow profile can be calculated theoretically. From the measurement of the particle velocity in such simple geometries, a relation between the mean particle and the mean fluid velocity is derived, which allows to obtain k_{por}. We also illustrated an alternative method based on the falling-head principle where we take advantage of the fact that the applied pressure and thus the particle velocity changes with a time constant depending on k_{por} as a function of time. For low-porosity structures with small flow rates, a constant-head measurement of Q is favourable, as it requires a much shorter measurement time. However, it also suffers from additional error contributions due to the reference measurement. For structures where a higher flow rate can be expected, the falling-head method is favourable, as the permeability can be deduced directly from the time dependence of $\bar{u}$. However, longer measurements are usually necessary.

Acknowledgments We would like to thank Valentin Blickle, Hans-Jürgen Kümmerer and Gerd E. Schröder-Turk for inspiring discussions.

Appendix 1: Theoretical calculation of mean particle velocity

First we assume that gravity leads to a non-uniform particle distribution described by the Boltzmann distribution

$$p(z) = e^{-z/\lambda}, \tag{4}$$

where λ is the gravitational length.

Second we use numerical values from (Staben et al. 2003) to describe the local particle velocity $u_d(z)$. Third we consider the biased sampling, as the inception rate of the

particles (coming from an infinite reservoir) is proportional to the particle speed, which results in an effective particle distribution

$$p_{\mathrm{eff}_d}(z) = u_d(z)p(z). \tag{5}$$

Combining these assumptions, the mean particle velocity is given by

$$\tilde{u}(d) = \frac{\int_{d/2}^{h-d/2} u_d(z)p_{\mathrm{eff}_d}(z)dz}{\int_{d/2}^{h-d/2} p_{\mathrm{eff}_d}(z)dz}. \tag{6}$$

Appendix 2: Exponential decrease in mean particle velocity

First we use that $\Delta P = \rho g \Delta h$ and the excess volume is given by $V = A_{\mathrm{res}}\Delta h$ which yields

$$V = \frac{A_{\mathrm{res}}\Delta P}{\rho g}. \tag{7}$$

Second we know the time derivative of the excess volume is related to the total flux, so that

$$\frac{d}{dt}V = 2Q, \tag{8}$$

where the factor 2 is due to the relative increase and decrease in the water column in the two reservoirs. Now we insert Eq. 7 and Darcy's law into Eq. 8, which gives

$$\frac{d}{dt}\Delta P = -\frac{2A\rho g k}{\eta L A_{\mathrm{res}}}\Delta P. \tag{9}$$

Using $\Delta P \propto \bar{u}$ we arrive at

$$\frac{d}{dt}\bar{u} = -\tau^{-1}\bar{u}, \tag{10}$$

where $\tau = \eta L A_{\mathrm{res}}/(2A\rho g k)$.

References

Auset M, Keller AA (2004) Pore-scale processes that control dispersion of colloids in saturated porous media. Water Resour Res 40(3):W03,503

Auset M, Keller AA (2006) Pore-scale visualization of colloid straining and filtration in saturated porous media using micromodels. Water Resour Res 42(12):W12S02

Bruus H (2007) Theoretical microfluidics. Oxford University Press, Oxford

Carman PC (1937) Fluid flow through granular beds. Trans Inst Chem Eng 15:150–166

Frenkel D (2002) Soft condensed matter. Phys A Stat Mech Appl 313(1–2):1–31. doi:10.1016/S0378-4371(02)01032-4

Katz AJ, Thompson AH (1986) Quantitative prediction of permeability in porous rock. Phys Rev B 34:8179–8181. doi:10.1103/PhysRevB.34.8179

Kozeny J (1927) Uber kapillare leitung des wassers im boden. Sitzber Akad Wiss Wien, Math-naturw 136:Abt. II a, p 277

Lindken R, Rossi M, Große S, Westerweel J (2009) Micro-particle image velocimetry ([small micro]piv): recent developments, applications, and guidelines. Lab Chip 9:2551–2567. doi:10.1039/B906558J

Loutherback K, Puchalla J, Austin RH, Sturm JC (2009) Deterministic microfluidic ratchet. Phys Rev Lett 102(4):045,301. doi:10.1103/PhysRevLett.102.045301

Marshall T, Holmes J, Rose C (1996) Soil physics. Cambridge University Press, Cambridge

Ouellette NT, O'Malley PJJ, Gollub JP (2008) Transport of finite-sized particles in chaotic flow. Phys Rev Lett 101(17):174,504. doi:10.1103/PhysRevLett.101.174504

Quake SR, Scherer A (2000) From micro-to-nanofabrication with soft materials. Science 290(5496):1536–1540. doi:10.1126/science.290.5496.1536

Sahimi M (1993) Flow phenomena in rocks: from continuum models to fractals, percolation, cellular automata, and simulated annealing. Rev Mod Phys 65(4):1393–1534. doi:10.1103/RevModPhys.65.1393

Santiago JG, Wereley ST, Meinhart CD, Beebe DJ, Adrian RJ (1998) A particle image velocimetry system for microfluidics. Exp Fluids 25:316–319. doi:10.1007/s003480050235

Segre G, Silberberg A (1962) Behaviour of macroscopic rigid spheres in poiseuille flow part 2. Experimental results and interpretation. J Fluid Mech 14(01):136–157. doi:10.1017/S0022112062001111

Staben M, Zinchenko A, Davis R (2003) Motion of a particle between two parallel plane walls in low-reynolds-number poiseuille flow. Phys Fluids 15:1711–1711

Taylor G (1953) Dispersion of soluble matter in solvent flowing slowly through a tube. Proc Royal Soc Lond Ser Math Phys Sci 219(1137):186–203. doi:10.1098/rspa.1953.0139

Pushkin DO, Melnikov DE, Shevtsova VM (2011) Ordering of small particles in one-dimensional coherent structures by time-periodic flows. Phys Rev Lett 106(23):234501-1–234501-4